# Numerical and experimental examination of the retention of magnetic nanoparticles in magnetic chromatography

Jan E. Marquardt [a,b,*], Carsten-Rene Arlt [c], Robin Trunk [a,b], Matthias Franzreb [c], Mathias J. Krause [a,b,d]

[a] *Lattice Boltzmann Research Group, Karlsruhe Institute of Technology, Karlsruhe, Germany*
[b] *Institute for Mechanical Process Engineering and Mechanics, Karlsruhe Institute of Technology, Karlsruhe, Germany*
[c] *Institute of Functional Interfaces, Karlsruhe Institute of Technology, Karlsruhe, Germany*
[d] *Institute for Applied and Numerical Mathematics, Karlsruhe Institute of Technology, Karlsruhe, Germany*

ARTICLE INFO

*Keywords:*
Lattice Boltzmann methods
Advection–diffusion equation
Euler–Euler approach
Multidimensional separation
Magnetic chromatography
OpenLB

ABSTRACT

This paper investigates a promising new approach of magnetic chromatography to improve particle fractionation in industrial-scale production. To understand the still challenging multidimensional separation mechanism, we develop a novel method to simulate magnetic nanoparticles' behavior in a magnetized chromatographic column based on a lattice Boltzmann method. In contrast to conventional numerical studies, the Euler–Euler approach is applied by utilizing the advection–diffusion equation to describe the particle component. As a result, the consideration of the magnetic force, the drag force, and a realistic diffusion are possible. Also, enormous computational costs are saved. We show that the column can be modeled from a combination of two unit cells, and a separation effect can be detected even with small magnetic fields. Furthermore, we compare the numerical results to practical experiments. Both results are in good accordance. We additionally determine potential improvements. Besides improving the setup by using stronger magnetic fields, the structure of the column's matrix plays an important role. Thus, we find that higher porosity leads to higher retention times.

## 1. Introduction

Technical nanoparticles are of increasing interest in novel therapeutic processes or the production of high quality products [1 3]. However, the synthesis of such nanoparticles shows an improvable homogeneity of the final products. For this purpose, fractionation processes are applied after production. Classical size fracturing processes reach their limits if industrially relevant quantities are to be provided since, in this size range, the physical separation principles used so far lose their effectiveness and selectivity. Established separation processes applicable in this size range, such as ultracentrifugation or ultrafiltration, provide mass flows on an analytical scale.

A novel approach for the size fractionation of nanoparticles is a magnetic chromatography mode, as explained in a recent work [4]. This technique consists of a method known from liquid chromatography. For this purpose, a stationary phase of steel spheres is formed, which serves as a separation matrix. Nanoparticles to be fractionated are passed through this separation matrix as a suspension in an aqueous mobile phase. By an external magnetic field, the matrix material can be magnetized to attract magnetic reactive nanoparticles. This separation technique is based on the fact that three forces acting on the nanoparticles are mainly responsible for the retention time in the separation matrix: the diffusion force, the drag force, and the magnetic force. By varying the particle size, the ratio of these forces can be shifted so that a change in the retention time occurs. This change can now be exploited to obtain a fractionation of nanoparticles. This process's functionality is shown in a present paper for nanoparticles with a diameter from 50 to 400 nm [4]. One advantage of such a chromatography method is the scalability, which can be achieved by varying the column length and thickness. For this scalability, however, a precise knowledge of the processes within the separation matrix is required. Therefore, a suitable method for a computer simulation is developed and used for the investigation.

In contrast to conventional liquid chromatography for molecular fractionation [5 7], magnetic chromatography has received little attention in numerical studies. Although there are methods that deal with similar processes, e.g., High Gradient Magnetic Separation (HGMS) utilizing wires [8,9], these examine significantly larger particles which are nonselectively separated and neglect diffusion. Thus, the proposed models do not represent all necessary mechanisms to model ultrafine particles' behavior in magnetic separation, as suggested by previous studies [10,11] and are, therefore, not suitable. Nevertheless, another method considers smaller, unresolved particles and diffusion in a two dimensional channel [12]. It was developed to deal with an application,

* Corresponding author at: Lattice Boltzmann Research Group, Karlsruhe Institute of Technology, Karlsruhe, Germany.
*E-mail address:* jan.marquardt@kit.edu (J.E. Marquardt).

also known as magnetic chromatography [13]. However, this system does not have a stationary phase within the fluid channel and is, for this reason, fundamentally different from the novel chromatography considered in this work, which utilizes a stationary phase consisting of spheres. Furthermore, this study also solely examines the separation of ultrafine particles, but not the suitability of such a system for size fractionation. Further development of this method considers HGMS with magnetic filter wires [14], but it examines simpler geometries than a pebble bed and is still only a two dimensional consideration.

Thus, it is still necessary to develop a method that describes the three dimensional shape of magnetized pebble beds and the resulting magnetic force on magnetic nanoparticles. Additionally, the method must represent these particles' diffusion and fluid convection in a physically correct way. All listed requirements are mandatory while performance is of utmost importance as we must consider high resolution 3D geometries due to large gradients and the chromatography column matrix's geometric properties.

In this work, we chose to meet the aforementioned requirements by solving the advection diffusion equation (ADE) and, therefore, using an Euler Euler approach. Because the ADE offers an established diffusion model and the computational effort only scales with the simulation domain's resolution. In contrast to this, an Euler Lagrange approach leads to a tremendous computational effort to achieve adequate accuracy by utilizing a sufficiently large number of particles [15,16].

We utilize lattice Boltzmann methods (LBM) for the ADE's solution because the parallelization is easy due to the costly computations being local [17], making it very well accessible for high performance computing, especially on parallel architectures [18]. LBM also work well to simulate multicomponent flows in complex geometries [17] and offer many other benefits [18]. For these reasons, we extend the approach previously presented by Trunk et al. [16] to observe a magnetic force stemming from several spheres of the ball matrix and that the simulation runs stable with an application of a realistic diffusion. Consequently, it is unnecessary to apply a larger diffusion coefficient or add artificial diffusion via numerical stabilization approaches, as discussed by John [19] and Augustine et al. [20], which would lead to deviations due to a non physical diffusion. The necessary novel method is developed utilizing the software package OpenLB [21,22].

This paper is structured as follows. In Section 2, we present the underlying mathematical equations, the Navier Stokes equation and the ADE. Furthermore, we explain the numerical methods utilizing LBM to solve these equations. Section 3 deals with the setup of the experiments under consideration. The corresponding results are listed and discussed in Section 4. Additionally, the results obtained by the practical and numerical experiments are compared. Finally, Section 5 summarizes and concludes this article.

## 2. Mathematical modeling and numerical methods

The physical process can be broken down into three different parts: the description of the two individual components, i.e., fluid and particles, and the coupling of these phases. Only one way coupling, which solely concerns the particle component, is considered. This procedure is adequate for the low particle concentrations used.

In the following, we describe the process divided into the individual components.

### 2.1. Fluid component

Since the fluid under consideration here is almost pure water, it is justified to use the incompressible Navier Stokes equation, which is given by

$$\rho_f \left( \frac{D\mathbf{u}_\mathrm{f}}{Dt} \right) = -\nabla p + \eta \nabla^2 \mathbf{u}_\mathrm{f} + \mathbf{f}, \tag{1}$$

where $\mathbf{u}_\mathrm{f}$ denotes the fluid velocity, $p$ the pressure, $t$ the time, $\mathbf{f}$ a body force, $\rho_\mathrm{f}$ and $\eta$ the fluid density and dynamic viscosity, to describe it.

Due to the flow through the ball matrix in the chromatography column, a pressure drop occurs. The Ergun equation [23], used to describe the pressure loss $\Delta p$ over the distance $L$, reads

$$\frac{\Delta p}{L} = \frac{150\eta}{4a^2} \frac{(1-\varepsilon)^2}{\varepsilon^3} \mathrm{u}_s + \frac{1.75\rho_f}{2a} \frac{1-\varepsilon}{\varepsilon^3} \mathrm{u}_\mathrm{s} \left|\mathrm{u}_\mathrm{s}\right|. \tag{2}$$

In this equation, $a$ is the radius of the uniformly sized spheres that form the chromatography matrix, $\varepsilon$ the void fraction and $\mathrm{u}_\mathrm{s}$ the superficial velocity.

The Boltzmann equation encompasses the incompressible Navier Stokes equation. Therefore, we solve it numerically by utilizing an LBM. However, as this article's focus is different, we refer to the relevant literature [18] for more in depth information.

The standard LBM with forces is utilized since it allows us to account for the pressure drop $\Delta p$ via a body force and thus obtain the velocity field within a pebble bed. Therefore, a source term $S_i$ related to the forces is needed in the lattice Boltzmann equation (LBE). Thus, following Guo et al. [24] the collision step can be written as

$$f_i^*(\boldsymbol{x}, t) = f_i(\boldsymbol{x}, t) + \left(\Omega_i(f) + S_i\right) \Delta t, \tag{3}$$

with the lattice location $\boldsymbol{x}$, the lattice time $t$, a collision operator $\Omega_i(f)$ and the particle populations before the collision $f_i$ as well as after it $f_i^*$. The streaming step, which reads

$$f_i(\boldsymbol{x} + \xi_i \Delta t, t + \Delta t) = f_i^*(\boldsymbol{x}, t), \tag{4}$$

where $\xi_i$ are discrete velocities, on the other hand, remains untouched. In this work, the Bhatnagar Gross Krook (BGK) collision operator [25] and a D3Q19 velocity set is chosen for the calculation of the fluid component. As a result of the former, the particle populations, $f_i$ relax towards their equilibrium $f_i^\mathrm{eq}$, at a certain rate. This rate is defined by the relaxation time

$$\tau_\mathrm{f} = 3\nu + \frac{1}{2}, \tag{5}$$

which can be calculated from the kinematic viscosity $\nu$.

Furthermore, periodical boundaries in each spatial direction are applied. The bounce back method, as shown by Ladd [26], is utilized to realize the macroscopic no slip boundary condition.

### 2.2. Particle component

The particle components description is analogous to the description by Trunk et al. [16], but we extend this consideration with the purpose that magnetic forces can be taken into account, and a stable simulation despite small diffusion coefficients is obtained.

To illustrate the procedure, we first go into the basic macroscopic equation, the advection diffusion equation, and give an overview of the forces the particles experience. Finally, we present how the problem is solved using the LBM.

#### 2.2.1. Advection diffusion equation

To calculate the distribution of the particle concentration $c$, we chose the advection diffusion equation, without sink nor source terms and assume that the diffusivity D is homogeneous:

$$\frac{\partial c}{\partial t} = \mathrm{D}\Delta c - \mathbf{u}_\mathrm{p} c, \tag{6}$$

with the particle velocity $\mathbf{u}_\mathrm{p}$. The latter can be calculated by the so called Stokes Einstein equation [27]:

$$\mathrm{D} = \frac{k_\mathrm{B} T}{6\pi\eta r_\mathrm{p}}, \tag{7}$$

where $k_\mathrm{B}$ is the Boltzmann constant, $T$ the temperature, and $r_\mathrm{p}$ the hydrodynamic radius of the diffusing particle.

### 2.2.2. Influences on particles

Apart from diffusion, other influences are decisive for the particle movement. While some forces, such as gravitational force and buoyancy, can be neglected due to the small particle size, the drag $F_{\mathrm{St}}$ and magnetic force $F_{\mathrm{m}}$, on the other hand, are among the competing forces. By considering these two forces, we can estimate the particle velocity by applying Newton's second law of motion, which in this case reads

$$m_{\mathrm{p}} \frac{D\mathbf{u}_{\mathrm{p}}}{Dt} = \boldsymbol{F}_{\mathrm{St}} + \boldsymbol{F}_{\mathrm{m}}, \tag{8}$$

with the particle mass $m_p$ and the forces mentioned above.

The nanoparticles are simplified considered as equally sized spheres. Therefore, we can utilize the Stokes drag force, which is given by

$$\boldsymbol{F}_{\mathrm{St}} = 6\pi\eta \left(\mathbf{u}_{\mathrm{f}} - \mathbf{u}_{\mathrm{p}}\right). \tag{9}$$

To describe the magnetic force acting on a particle of the volume $V_{\mathrm{p}}$ caused by a sphere with radius $a$, which is uniformly magnetized by an external magnetic field with constant intensity $H_0$, we use the following equation:

$$\boldsymbol{F}_{\mathrm{m}} = V_{\mathrm{p}}\mu_0 \Delta\chi \times \begin{pmatrix} -\frac{a^3 \boldsymbol{M}_{\mathrm{s}}}{r^4}\left[2\left(\boldsymbol{H}_0 + \frac{2a^3}{3r^3}\boldsymbol{M}_{\mathrm{s}}\right)\cos^2\theta + \left(-\boldsymbol{H}_0 + \frac{a^3}{3r^3}\boldsymbol{M}_{\mathrm{s}}\right)\sin^2\theta\right] \\ 0 \\ \frac{\cos\theta\sin\theta}{r}\left[-\left(\boldsymbol{H}_0 + \frac{2a^3}{3r^3}\boldsymbol{M}_{\mathrm{s}}\right)^2 + \left(-\boldsymbol{H}_0 + \frac{a^3}{3r^3}\boldsymbol{M}_{\mathrm{s}}\right)^2\right] \end{pmatrix}_{(r,\phi,\theta)}, \tag{10}$$

as reported by Ebner et al. [28]. For the equation, a spherical coordinate system with the origin at the center of the sphere and coordinates $r$, $\phi$, and $\theta$ is utilized. According to Franzreb [29] the difference between the magnetic susceptibilities of the particle and the fluid is $\Delta\chi \approx 3$ for low magnetic field strengths. The vacuum permeability is called $\mu_0$ and is also included in the equation used to calculate the magnetic field strength from the magnetic flux density $B_0$, which reads

$$\boldsymbol{H}_0 = \mu_0 \mu_r \boldsymbol{B}_0. \tag{11}$$

There is also a dependence on the magnetic permeability $\mu_r$. Here, $\mu_r \approx 1$ applies because we solely consider water. Through the utilization of this, the magnetization of spheres can be approximated by [29]

$$\boldsymbol{M}_{\mathrm{s}} = \begin{cases} \boldsymbol{M}_{s,S}, & \boldsymbol{H}_0 \geq \boldsymbol{M}_{s,S}/3 \\ 3\boldsymbol{H}_0, & \boldsymbol{H}_0 < \boldsymbol{M}_{s,S}/3 \end{cases}. \tag{12}$$

The saturation magnetization $\boldsymbol{M}_{\mathrm{s,S}} \approx (0, 0, 6.2)^{\mathrm{T}} \cdot 10^5$ A/m is utilized, which is a result of measurements. For the sake of simplicity, we assume that particles do not accumulate on the magnetized spheres and, therefore, do not affect the shape or magnetic properties of the ball matrix. This assumption leads to negligible errors since only a low particle concentration, and a small magnetic field are considered.

### 2.2.3. Numerical consideration

With the LBM, advection diffusion problems can also be solved. Since we only use it for a scalar quantity, the particle concentration, it is sufficient to utilize a reduced lattice [30,31]. Therefore, in this work, the D3Q7 velocity set is chosen for the particle component, which saves further computational effort. The LBE, which reads

$$g_i(\boldsymbol{x} + \xi_i \Delta t, t + \Delta t) = g_i(\boldsymbol{x}, t) + \Omega_i(g)\Delta t, \tag{13}$$

with the density distribution functions $g_i$, can be used for the particle phase. Merely the collision operator $\Omega_i(g)$ changes, since the equilibrium distribution function $g_i^{\mathrm{eq}}$ and the relaxation time differ. The latter depends in this case on the lattice diffusivity $D$:

$$\tau_{\mathrm{p}} = 3D + \frac{1}{2}. \tag{14}$$

However, the obtained solutions depend on $\tau_{\mathrm{p}}$, and using a small lattice diffusivity yields errors [32] and instability [33]. This problem, we too experience in this work, as the diffusion coefficient $D$ is always small compared to the viscosity $\nu$, since there is a difference of several orders of magnitude. For this reason, we choose the two relaxation times (TRT) collision operator [34] instead. The TRT model is similar to the BGK collision operator, but it uses two different relaxation times, one for the symmetric $\tau_{\mathrm{p}}^{+}$ and one for the antisymmetric parts $\tau_{\mathrm{p}}^{-}$. Both times are linked by

$$\Lambda = \left(\frac{\tau_{\mathrm{p}}^{+}}{\Delta t} - \frac{1}{2}\right)\left(\frac{\tau_{\mathrm{p}}^{-}}{\Delta t} - \frac{1}{2}\right), \tag{15}$$

which is now decisive for the stability and accuracy of the simulation [32] and through which $\tau_{\mathrm{p}}^{+}$ can be freely chosen, since $\tau_{\mathrm{p}}^{-} = \tau_{\mathrm{p}}$, see (14). We choose $\Lambda = 1/4$, as it leads to the most stable simulations [35].

By applying a forward Euler scheme for the temporal discretization of (8), we can determine the particle velocity after a time step with

$$\mathbf{u}_{\mathrm{p}}(\mathbf{x}, t + \Delta t^*) = \left(\mathbf{u}_{\mathrm{p}} + \Delta t^* \left(\frac{\boldsymbol{F}_{\mathrm{St}} + \boldsymbol{F}_{\mathrm{m}}}{m_{\mathrm{p}}} - \mathbf{u}_{\mathrm{p}} \cdot \nabla \mathbf{u}_{\mathrm{p}}\right)\right)(\mathbf{x}, t). \tag{16}$$

For calculating the velocity gradient $\nabla \mathbf{u}_{\mathrm{p}}$, we utilize a classical upwind scheme as outlined by Courant et al.[36].

At this point, it is crucial to note that the time step $\Delta t^*$ used here can be the same as the one utilized in the LBM, but does not have to be. This is because the drag force causes a relaxation of the particle velocity $\mathbf{u}_{\mathrm{p}}$ to the fluid velocity $\mathbf{u}_{\mathrm{f}}$ and if the associated factor of this relaxation $6\pi\eta\Delta t^*/m_{\mathrm{p}} > 1$, then an over relaxation takes place. Since we are looking at nanoparticles, this is the case in this study, so we choose $\Delta t = n\Delta t^*$, for $n \in \mathbb{N}_{>0}$, and perform the calculation of the velocity $n$ times in each lattice time step $\Delta t$. However, this causes enormous calculation costs. Thus, we refrain from the calculation as soon as we obtain the stationary solution. We assume that the stationary solution is reached when the particle velocity field's relative error is less than 0.001%.

Analogous to Trunk et al. [16] we use a Dirichlet boundary condition with a fixed particle concentration for the inlet and a Neumann boundary condition for the outlet. Besides, on the ball surfaces, we use the bounce back rule to describe the no slip condition.

### 2.2.4. Algorithm

For clarification, we present the basic utilized algorithm, which uses the methods mentioned previously, in Algorithm 1. Particularly noteworthy is the separate calculation of the fluid and particle solution, as well as the change of the temporal discretization possible through it. Additionally, it must be emphasized that the algorithm uses sub time steps to calculate particle velocities, see Section 2.2.3.

**Algorithm 1:** Basic, simplified algorithm used to solve the proposed problem.

```
initialization;
// Calculation of stationary fluid solution
for all time steps do
    collision & streaming;
end
change of time discretization;
// Calculation of particle solution
magnetic force calculation;                          ▷ See Eq. (10)
for all time steps do
    if not stationary then
        drag force calculation;                      ▷ See Eq. (9)
        for all n sub steps do
            particle velocity field calculation;     ▷ See Eq. (16)
        end
    end
    collision & streaming;
end
```

**Table 1**
Comparison of the calculated magnetic force with the implemented method $\mathbf{F}_m$ and the result of an external calculation $\mathbf{F}_m^*$, specifying the position $\boldsymbol{x}$ in Cartesian coordinates, which has its origin in the center of the uniformly magnetized sphere.

| $\boldsymbol{x}$ in m | $\mathbf{F}_m$ in N | $\mathbf{F}_m^*$ in N |
|---|---|---|
| $\begin{pmatrix} 0.01 \\ 0.01 \\ 0.01 \end{pmatrix}$ | $\begin{pmatrix} 2.4094206 \\ -4.5149362 \\ -1.0527578 \end{pmatrix} \cdot 10^{-10}$ | $\begin{pmatrix} 2.4094206 \\ -4.5149362 \\ -1.0527578 \end{pmatrix} \cdot 10^{-10}$ |
| $\begin{pmatrix} -0.01 \\ -0.01 \\ 0.01 \end{pmatrix}$ | $\begin{pmatrix} -2.4094206 \\ 4.5149362 \\ -1.0527578 \end{pmatrix} \cdot 10^{-10}$ | $\begin{pmatrix} -2.4094206 \\ 4.5149362 \\ -1.0527578 \end{pmatrix} \cdot 10^{-10}$ |
| $-\begin{pmatrix} 0.02 \\ 0.02 \\ 0.02 \end{pmatrix}$ | $\begin{pmatrix} 0.20799102 \\ -0.19154168 \\ 0.0082246703 \end{pmatrix} \cdot 10^{-10}$ | $\begin{pmatrix} 0.20799102 \\ -0.19154168 \\ 0.0082246703 \end{pmatrix} \cdot 10^{-10}$ |

**Table 2**
Comparison of the analytical $\boldsymbol{u}_\mathrm{p}^*$, calculated using (17), and numerical solution $\boldsymbol{u}_\mathrm{p}$. In addition, the applied constant magnetic force $\boldsymbol{F}_\mathrm{m,c}$ used is shown. The calculation parameters and results are the same for each spatial direction.

| $F_\mathrm{m}^\mathrm{c}$ in N | $\mathrm{u}_\mathrm{p}$ in m/s | $\mathrm{u}_\mathrm{p}^*$ in m/s |
|---|---|---|
| $5.65486678 \cdot 10^{-9}$ | 0.0333333333 | 0.0333333333 |
| $5.65486678 \cdot 10^{-7}$ | 3.33333333 | 3.33333333 |
| $5.65486678 \cdot 10^{-5}$ | 333.333333 | 333.333333 |

#### 2.2.5. Verification

The previously mentioned methods are validated in advance em ploying a few small tests. These tests show that the forces are precisely calculated and that they are correctly applied.

In the first test, the evaluation of the magnetic force, see (10), in the software used, is compared with externally calculated results. Results consistent with the comparative data are obtained. Varying parameters like the positions, magnetic field intensity, and sphere diameter always lead to relative errors smaller than $10^{-7}$ %. As an example, we present one of the fictitious test setups and some of the retrieved results. In this setup, the uniformly magnetized sphere has a radius of 1 cm and the magnetic particles have a radius of 10μm. Additionally, we utilize a magnetic field strength $H_0$ of 30 000 A/m and the sphere magnetization $M_s = 3H_0$. A small extract of the results is shown in Table 1.

In the second test, we regard the particle velocity, to check the realization of (16) and its application to confirm that the forces are rightly applied. Using a force equilibrium of the Stokes drag and a constant magnetic force $\boldsymbol{F}_\mathrm{m}^\mathrm{c}$ we obtain

$$\mathbf{u}_\mathrm{p} = \frac{\boldsymbol{F}_\mathrm{m,c}}{6\pi\eta r_\mathrm{p}}, \tag{17}$$

as the analytical solution of the problem. We look at different setups and scenarios to compare this analytical solution with the simulation. For these test cases, parameters vary independently from each other, e.g., magnetic force $\boldsymbol{F}_\mathrm{m}^\mathrm{c}$ and particle size $r_\mathrm{p}$. In Table 2, we show a small extract of the tests obtained for a kinematic viscosity of $9 \cdot 10^{-7}$ m$^2$/s, a fluid density of 1000 kg/m$^3$, a particle radius of 10 μm and density of 2000 kg/m$^3$. As it turns out, the results are in excellent agreement.

Therefore, the tests show that the methods described above give correct results, taking the simplifications into account.

## 3. Experiments

### 3.1. Practical experiment

#### 3.1.1. Experimental setup

A self developed process is used for the chromatographic concept in this work. For this purpose, a glass chromatography column was equipped with a stationary phase consisting of steel spheres [4]. Spher ical matrix materials are widely used in liquid chromatography due to their advantageous surface ratio and uniform packability [37,38]. For this matrix material, a stainless steel powder, TruForm 174 of the company Praxair Surface Technologies, Ratingen, Germany fabricated for 3D selective laser melting (SLM) was used. The particles consist of a chromium rich (12.5%) alloy with a small amount of carbon, silicon, and manganese. Their particle size distribution ranges from 5 to 50 μm with a D50 value of 31 μm. In secondary electrode microscopy images, good sphericity could be determined. The particles show a high satu ration magnetization of 150 A m$^2$/kg, a remanence of 95 mA m$^2$/kg, and a coercivity of 160 A/m. Due to its low remanence, this column material shows no relevant residual magnetization, even after several magnetizations.

The magnetic field source is a Helmholtz coil arrangement including four larger coils with an inside diameter of 3 cm and an outside diame ter of 4.6 cm placed in an adjusted distance to each other to generate a nearly homogeneous field in the center of the arrangement. The outer coils had 300 windings, while the inner coils had 172 windings. By using this set up, a magnetic field can be generated, increasing linearly with the current intensity. With a current of 125 mA a magnetic field of 0.85 mT was generated. The necessary current was supplied by a laboratory power supply unit (Distrelec Group AG, Uster, Switzerland), which could supply voltages of up to 30 V and currents of up to 5 A. The chromatography set up used for this work, consists of a borosilicate glass column (Diba Industries Inc., Danbury, Connecticut) with a bed length of 110 mm and an inner diameter of 6.6 mm. One PTFE frit at the beginning and end of the column with a pore size of 5 μm served as a filter to retain the matrix material and exclude larger impurities.

For all liquid handling, an FPLC (Fast Protein Liquid Chromatogra phy) system (Äkta purifier, GE Healthcare, Buckinghamshire, England) is used, which is equipped with PEEK capillaries with an inner diameter of 0.25 m. The laboratory setup is shown in Fig. 1. A sample is injected into the system using a six port diaphragm valve, defining the volume via a connected loop. Here a loop of 500μL is selected. A constant flow rate of 2.44 mL/min is used. The liquid leaving the column is analyzed online with a UV cell at 280 nm and a conductivity cell, which are both included in the FPLC system. If the effluent has to be collected for size analysis, a fraction collector could be used. In this experimental series, breaking points of 250 mL are chosen. A 1 mM Tris (Carl Roth GmbH, Karlsruhe, Germany) buffer with a pH value of 9.5 guarantees a stable, disperse system. Therefore, it is used as the mobile phase. After each experimental run, the column is flushed with buffer without applying a magnetic field to remove any residual material.

#### 3.1.2. Experimental procedure

All columns used are packed under a uniform method. Since the ma terial shows fast settling rates due to its high density, discrete amounts of slurry are pipetted into the column with a fast pump pulse to avoid sedimentation related layering. The separation matrix is finalized under a flow of 10 mL/min for 15 min. The quality of the separation column packing is controlled by injecting a tracer peak of 1% (v/v) aqueous acetone solution and measuring its asymmetry through the resulting UV signal. The quality of the column packing is defined as acceptable within an asymmetry range of 1 1.4. If the asymmetry is outside of this range, the column is repacked. In the process of a particle retention experiment, first, the separation column is equilibrated at a flow rate of 4 mL/min with 10 mL (according to 3 full column volumes) of Tris buffer at a magnetic field of 0 mT in order to remove residual nanoparticles from the previous experiment. Afterward, the required magnetic field is adjusted by the current of the power source. A pulse of 500μL of the nanoparticle suspension is injected at the same flow rate, and the pumping of the solvent is continued until the UV Signal in the effluent reaches its baseline level again. The sample solution contains 40 mg/mL maghemite nanoparticles. This concentration difference is chosen because the maghemite particles show an intensive absorption and therefore, peaks of comparable size are produced. Before use, the resulting nanoparticle sample is diluted in the running buffer and retitrated to a pH of 9.5 immediately before use to eliminate the

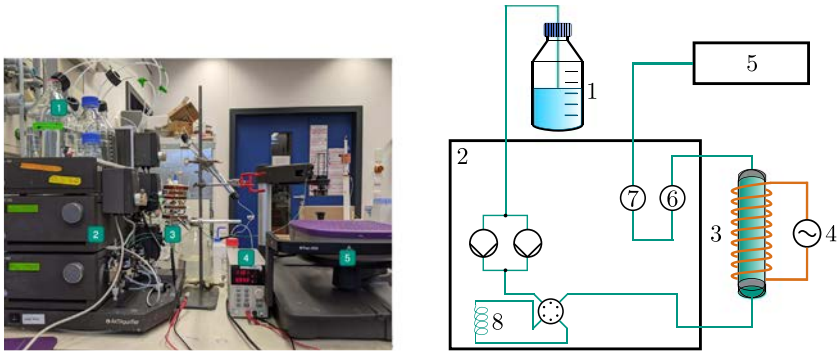


**Fig. 1.** Experimental setup for the magnetic chromatography fractionation process (left) and respective process scheme (right). 1: Process solution reservoirs; 2: Fast Protein Liquid Chromatography (FPLC) handling station; 3: Chromatography column embedded in a Helmholtz coil setup; 4: Laboratory power supply unit; 5: Fraction collector; 6: UV cell; 7: Conductivity cell; 8: Sample injection loop.

influences of the particles' storage buffer. In the case of experiments with magnetic field application, the magnetic field is switched off after 4.5 mL to remove any magnetically bound particles, which corresponds to a time of 1.84 min.

### 3.1.3. Analytical procedures

The particle size distribution of the magnetic nanoparticles is determined using the dynamic light scattering measured with a Zetasizer (Zetasizer Nano ZSP, Malvern Instruments, Malvern, England) with a detection range between 0.1 nm and 10 µm. The measurement value is the intensity size distribution. The fractionation samples are used for this purpose. Particle size determination is carried out in triplicates. For process technical reasons, each fraction from the chromatographic separation consists of a size distribution. In order to define a fixed elution time for a particle size, the respective proportions of a particle size are calculated and weighted according to the peak area fraction of the fraction. The elution time is determined when 50% of the respective particle size left the column.

As model particles, Synomag D (Micromod Partikeltechnologie GmbH, Rostock, Germany) particles are used. These are core shell particles with a maghemite core surrounded by a dextran shell and have superparamagnetic properties. According to the manufacturer, the particles have a nominal hydrodynamic diameter of 50 nm. With Dynamic Light scattering measurements, this particle sample is analyzed. A size range of 20 to 70 nm is determined. The core shell particles have a saturation magnetization of 48 A $m^2$/kg. The stock solution consists of 25 mg/mL and is diluted for the respective experiments with Tris buffer.

## 3.2. Numerical experiment

In order to reduce the computational effort, the ball matrix is modeled from two unit cells, namely primitive cubic (cP) and body centered cubic (cI). This choice was made because the porosities of these two cells ($\varepsilon_{cP} = 0.476$, $\varepsilon_{cI} = 0.32$) are the closest to the real one ($\varepsilon_B = 0.42$). The entire length of the column can be described by approximately 2350.84 cP and 1316.47 cI cells. As a result, the porosity of the real ball matrix is also achieved on average. Both cubic unit cells are shown in Fig. 2.

Since the particle component does not influence the fluid, it can be considered independently. Accordingly, it is evident that the fluid velocity field has only constant influences and is, therefore, stationary. For this reason, to save computational effort and, more importantly, to further stabilize the calculations, the simulations are divided for the solution of the fluid and the particles. This segmenting allows us to use different time steps $\Delta t_f$ and $\Delta t_p$ to adjust the relaxation times, so that more stable and accurate results can be provided. Table 3 shows the setup used for the respective components and unit cells. Due to the lower porosity of the cI cell, higher velocity is achieved and, therefore, a stable simulation is more difficult to achieve. The problem was solved by further refinement of the mesh.

**Table 3**
Used setup for different cubic unit cells and phases.

| Component | Lattice spacing $\Delta x$ in m | Time step $\Delta t$ in s | Relaxation time $\tau$ |
|---|---|---|---|
| Fluid | $2.5 \cdot 10^{-7}$ | $1.0 \cdot 10^{-8}$ | 0.928442 |
| Particle (25 nm) | $2.5 \cdot 10^{-7}$ | $3.125 \cdot 10^{-6}$ | 0.50193 |
| Particle (50 nm) | $2.5 \cdot 10^{-7}$ | $3.125 \cdot 10^{-6}$ | 0.500965 |

**Table 4**
Simulation parameters used.

| Symbol | Description | Value | Unit |
|---|---|---|---|
| $\rho_f$ | Density of water | 997.1 | kg $m^{-3}$ |
| $\eta$ | Dynamic viscosity of water | $8.9 \cdot 10^{-4}$ | Pa s |
| $T$ | Temperature | 293.15 | K |
| $\beta_0$ | Injected mass concentration of particles | 0.25 | g $L^{-1}$ |
| $\Phi_{min}$ | Minimal volume fraction of particles | $10^{-8}$ | – |
| $a$ | Radius of the spheres of the matrix | 15.5 | µm |
| $t_{max}$ | Maximal simulated time period | 20 | s |
| $t_i$ | Time between measurements | 0.1 | ms |
| $\Delta t_{in}$ | Time period of injection | 5 | ms |

Since only one particle size can be considered per simulation, representative particle sizes for the practical experiment, particularly nanoparticles with radii of 25 and 50 nm, are numerically investigated. These examined particles have a density of 2500 kg/$m^3$ and are considered as perfect spheres. In addition, the saturation magnetization $M_{p,S} \approx 9.1 \cdot 10^3$ A/m according to the manufacturer's specifications is taken into account.

The parameters of the simulation are listed in Table 4. However, some parameters could not be reproduced exactly as in practical experiments. For instance, the injection time had to be decreased, because we are only looking at a fraction of the total length. Otherwise, with a longer injection time, some particles would already leave the domain, which would falsify the result. In reality, the inlet's concentration profiles vary. To counteract this, we have now chosen a uniform profile with a concentration $\beta_0$. Additionally, the fluid is only considered as pure water, as the small proportion of foreign substances is negligible. A maximum period of 20 s is regarded. If the relative change of the particle concentration every 5 ms is less than $10^{-8}$ %, the simulation is stopped earlier.

Comparability is ensured by using the mean transit time $\bar{t}_t$ to describe the retention's strength. According to Levenspiel [39], it can be calculated, assuming zero background concentration, for pulse experiments by

$$\bar{t}_t = \frac{\int_0^\infty tC\,dt}{\int_0^\infty C\,dt} \approx \frac{\sum_i t_i C_i \Delta t_i}{\sum_i C_i \Delta t_i}, \tag{18}$$

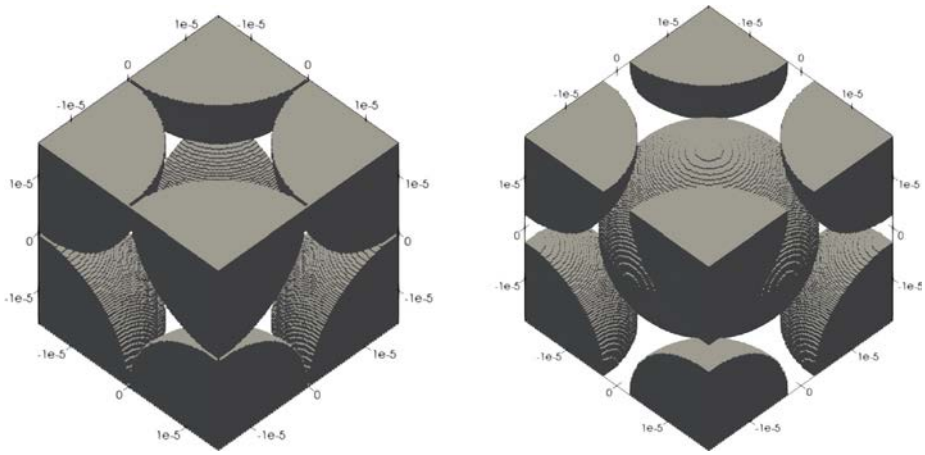

**Fig. 2.** Illustration of cubic unit cells, namely primitive cubic (left) and body-centered cubic (right), which are used to (roughly) describe a chromatographic column, with additional representation of the calculation grid. Length specifications are in meters.

where $t$ is the time passed since the instantaneous introduction of nanoparticles and $C$ the concentration at the outlet. The index $i$ stands for the discrete measurements performed in our numerical experiments at the time $t_i$ every $\Delta t_i = 0.1$ ms. All values until the end of the simulation are summed up, which is the case at $t_{\max}$ at the latest.

## 4. Results and discussion

### 4.1. Experimental results

The chromatography column is analyzed using tracer experiments. A void volume of 1.65 mL is determined, which equals a retention time of 33 s at a flow rate of 2.44 mL/min. The total porosity of the column is, therefore, 0.42. By using the UV signal of the chromatographic procedure, the flow retention of the nanoparticles without an external magnetic field and at 0.85 mT can be observed in Fig. 3 (left). It can be observed that after switching off the magnetic field, a UV increase occurs. This indicates that some of the nanoparticles are temporarily bound by the magnetic field and are released when the magnetic field is switched off. Furthermore, a later rise in the peak can be observed as well as an increased tailing. Peak broadening effects can explain this due to the magnetic field, which has already been observed in previous work [4]. The peak is divided into individual fractions with the aid of a fractionator. The respective segments can also be seen in the chromatogram.

The DLS analyses of the individual fractions each showed particle size distributions of the nanoparticles with a percent error from 1.3 to 3.6%. Fig. 3 (right) shows an example of the result of such a measurement. Here it can be seen that even later elution times contain discrete amounts of smaller particle sizes. Several factors make a real separation difficult. Especially in this experimental setup, this is not an ideal ball packing of the separation matrix. Due to the size distribution of the matrix from 5 to 50µm, irregularities may occur, which reduces the separation performance. Besides, further process relevant factors like a longitudinal diffusion of the nanoparticles are in the periphery of the FPLC system. However, if examining the average size distribution of the fractions, it can be seen that the D50 values increase throughout the process. This, in turn, suggests the expected increased retention of larger nanoparticles within the separation matrix. Subsequently, the respective UV surfaces of the peak fractions are integrated. Based on the DLS data, the respective proportion of the particle size was determined. Thus, the elution behavior of different particle sizes was tracked. For comparability with the numerical results, an elution time is required. To obtain this in the experimental results, the time was determined when 50% of the respective particle size was eluted again. The elution

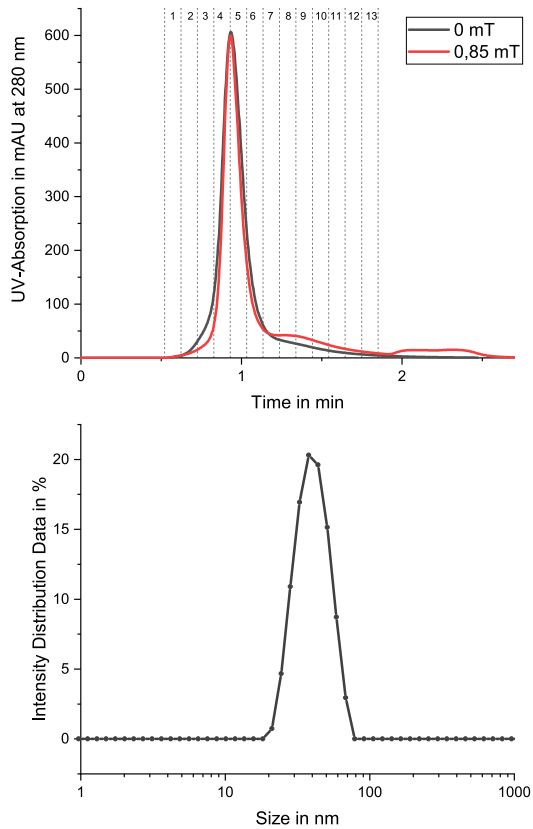


**Fig. 3.** Top: Chromatograms of particle separation with 0.85 mT and without magnetic field. The UV signal is plotted over the experimental time. The division of the graph shows the fractionation of the leaving solution. Bottom: Exemplary Dynamic Light Scattering measurement of an experimental fraction by intensity. The percentage is plotted over the size.

times determined in this way for the particle sizes under consideration can be seen in Table 5.

Based on the results, it can be seen that an elution difference is already present in an experimental procedure without applying a mag netic field. This difference could indicate the maghemite nanoparticles' spontaneous magnetization, which already creates a magnetic interac tion with the matrix material. This effect could already be observed in

**Table 5**
Listing of the experimental and numerical results for different setups.

| Magnetic field | Particle size | Mean transit time | | Relative error |
|---|---|---|---|---|
| | | Experiment | Simulation | |
| 0 mT | 25 nm | 52.32 s | 54.94 s | 5.01% |
| | 50 nm | 55.80 s | 54.80 s | −1.80% |
| 0.85 mT | 25 nm | 54.12 s | 55.04 s | 1.70% |
| | 50 nm | 57.12 s | 55.43 s | −2.94% |

**Table 6**
Utilized lattice setup for the study of the grid independence for a particle radius of 5 nm and a magnetic flux density of 5 mT.

| Resolution | Phase | Lattice spacing $\Delta x$ in m | Time step $\Delta t$ in s |
|---|---|---|---|
| 16 | Fluid | $1.9375 \cdot 10^{-6}$ | $6.0 \cdot 10^{-7}$ |
| | Particle | | $5.0 \cdot 10^{-5}$ |
| 32 | Fluid | $9.6875 \cdot 10^{-7}$ | $1.5 \cdot 10^{-7}$ |
| | Particle | | $1.25 \cdot 10^{-5}$ |
| 64 | Fluid | $4.84375 \cdot 10^{-7}$ | $3.75 \cdot 10^{-8}$ |
| | Particle | | $3.125 \cdot 10^{-6}$ |
| 128 | Fluid | $2.421875 \cdot 10^{-7}$ | $9.375 \cdot 10^{-9}$ |
| | Particle | | $7.8125 \cdot 10^{-7}$ |

a previous work [4]. Here, however, it can be seen that larger particles are more strongly affected by this effect than smaller ones. Therefore, separation, according to particle size, is possible. The application of a weak magnetic field of 0.85 mT to the experiment increases the elution times of both particle sizes. These investigations show the magnetic influence on the separation process. The retention time varies according to particle size, whereby the retention of the larger nanoparticle variant is greater again. This observation also confirms the hypothesis that the magnetic interaction of the nanoparticles with the separation matrix is beneficial to obtain the purification of very fine particles.

### 4.2. Numerical results

In the following, we first consider grid independence before we go on to discuss the results of the numerical analysis of a chromatography column.

#### 4.2.1. Grid independence

The cP case is utilized for confirmation of the grid independence. A coarse resolution is necessary since otherwise, calculation inaccu racies due to machine epsilons and calculation effort increase too significantly. Therefore, we consider 5 nm particles to achieve a stable simulation. For this reason, the magnetic induction is also increased to 5 mT. Also, the simulated period is increased to 10 s. We consider the lattices as they are given in Table 6 with a diffusive scaling. For comparison, we regard the relative error $\epsilon$ of the mean transit time $\bar{t}_t$, which is calculated as follows:

$$\epsilon(N) = \frac{\bar{t}_t(N) - \bar{t}_t(N_{max})}{\bar{t}_t(N_{max})}, \tag{19}$$

with $N$ being the resolution, which is chosen to be 16, 32 or 64. An analytical solution is not available. Therefore, a simulation with a resolution of $N_{max} = 128$ is used to calculate the error instead.

In Fig. 4 the relative error is shown over the simulation resolution. A sublinear convergence is apparent, as a result of a large number of curved boundaries. The spheres are sometimes over or underestimated and, in the former case, may even cut off the areas with high magnetic forces.

#### 4.2.2. Chromatography column

Figs. 5 and 6 show the calculated fluid velocity fields and magnetic forces for nanoparticles with a diameter of 50 nm for the cP and cI

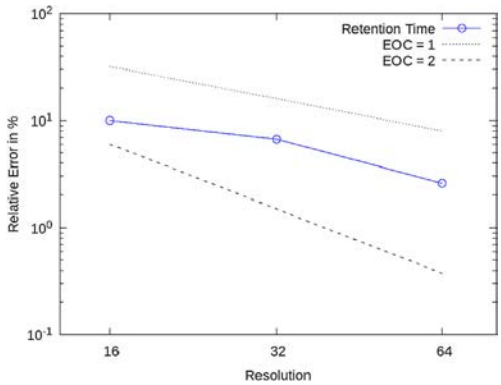


**Fig. 4.** Relative error $\epsilon$ versus the system resolution $N$.

**Table 7**
Listing of the numerical results for the individual cubic unit cells.

| Cell | Magnetic induction $B_0$ | Particle radius $r_p$ | Mean transit time $\bar{t}_t$ |
|---|---|---|---|
| cP | 0.00 mT | 25 nm | 16.16 ms |
| | | 50 nm | 16.12 ms |
| | 0.85 mT | 25 nm | 16.19 ms |
| | | 50 nm | 16.35 ms |
| cI | 0.00 mT | 25 nm | 12.88 ms |
| | | 50 nm | 12.84 ms |
| | 0.85 mT | 25 nm | 12.89 ms |
| | | 50 nm | 12.92 ms |

cases. In areas of high fluid velocity, there is a low magnetic force and vice versa. Furthermore, one can see that the body centered cubic unit cell has deflections, whereas, in the primitive cubic cell, the fluid mainly flows through its center. However, there is a larger channel for the fluid in the cP case. For this reason, we observe a significantly lower fluid velocity.

For the quantification of the results, the mean transit time of the individual unit cells is first considered. These results are shown in Ta ble 7. It is visible that the particles already remain longer in the domain when a small magnetic force is applied. Also, we see that the magnetic force's influence grows stronger, with bigger particles. Furthermore, we find out that the retention in the body centered cubic is minor compared to the primitive cubic, although its edges are longer. The notably different fluid velocity causes this difference. We additionally see that the smaller 25 nm particles experience longer retention than the 50 nm particles without applying a magnetic field. The cause for this is that the smaller particles experience stronger diffusion and less drag force. Therefore, the diffusion becomes more competitive, leading to a higher particle concentration in areas with a lower fluid velocity. We also see that the application of an already weak magnetic field negates this effect since the magnetic force's influence is more significant.

By describing the length and porosity of the chromatography col umn through these two cubic unit cells, see Section 3.2, the mean transit times, as shown in Table 5 are obtained. A minor influence of the magnetic force is once again visible. Additionally, we notice that larger nanoparticles experience a greater magnetic force and are retained longer than smaller ones.

### 4.3. Comparison and discussion

Table 5 compares the numerical as well as experimental results and shows a relative error, which is calculated analogously to (19). The numerical and experimental investigations both provide results in the same order of magnitude and only a minor effect of a weak magnetic field. The absolute value of the relative error is always less than 3%, with one exception. For the observation of the 25 nm particles without

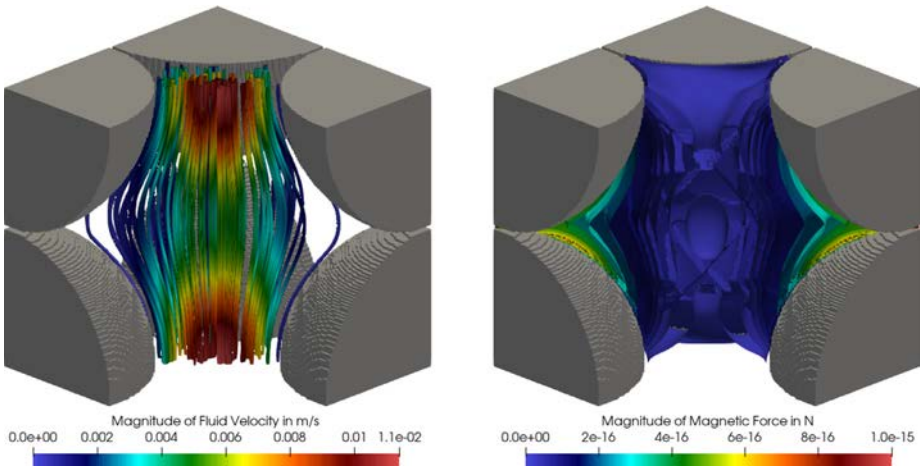


**Fig. 5.** Representation of the velocity (left) and magnetic force (right) within the primitive cubic unit cell.

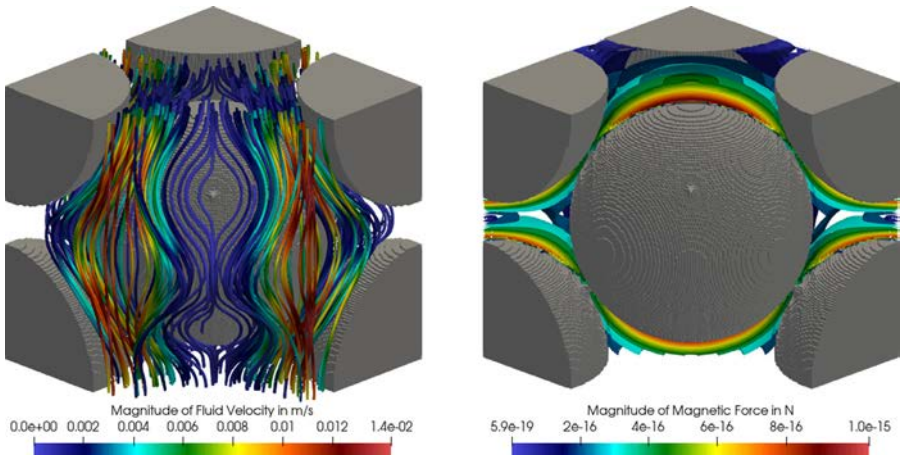


**Fig. 6.** Visualization of the body-centered cubic unit cell showing the velocity (left) and the magnetic force (right).

the magnetic field, a relative error of about 5.01% is observed. This increment can be explained above all by the spontaneous magnetization of the nanoparticles. Particles of around 20 to 70 nm are too large to be superparamagnetic but instead form single domain bodies in which the atomic magnetic moments are aligned, resulting in a spontaneous magnetization of the nanoparticles [40]. At a macroscopic scale, the spatial orientation of the particles and the corresponding magnetization are randomly distributed, which leads to mutual extinction. However, when individual nanoparticles interact with magnetizable macroscopic bodies, the spontaneous magnetization leads to an attractive force and corresponding retention in the experimental structure, which is not considered in the simulations. Additionally, errors in all deviations are caused by the simplifications used for the numerical consideration, e.g., the representation of the ball matrix as unit cells consisting of perfect spheres, which only describe reality up to a certain degree. The applied uniform concentration profile leads to minor deviations as well. Also, errors are expected due to a rather coarse temporal resolution in the measurements and inaccuracies and errors of the instruments.

Finally, we observe for both cases that the magnetic field influences larger particles more strongly, although the difference is only small. Thus, the influence of the applied magnetic field is only minor with this setup. This minor effect becomes clear by regarding the difference in the retention times with and without a magnetic attraction force. In both cases, the absolute difference is approximately the same. However, the numerical experiments provide detailed knowledge on a different size scale. These findings are otherwise hardly tangible, like under standing the dynamics in the vicinity of the magnetized spheres in the matrix.

A more significant retention difference is obtainable through an increment of the magnetic flux density since the magnetic attraction depends on the particle volume, see (10). This increment is a straight forward improvement. However, the magnetic particles are not to be retained indefinitely inside the column. Therefore, it comes down to a balancing act to find an optimized magnetic flux density. The developed numerical method has the potential to perform optimizations like this significantly more economically than practical experiments.

Furthermore, the numerically conducted studies show a new area for improvement, namely matrix optimization. On the one hand, sig nificant areas show small field gradients, limiting the efficiency of the process. In order to improve this efficiency, selecting a matrix material with enhanced properties and reducing the low gradient ar eas are beneficial. The latter is possible by optimizing the matrix components' shape and lowering the matrix's porosity. On the other hand, the observations show that only an increase in porosity at a constant volume flow rate leads to an improvement in separation due to the drag force's influence. Thus, it comes again down to a balancing act searching for optimal matrix parameters to increase fractionation efficiency. The studies conducted suggest that further optimization of the stationary phase is relevant under the current conditions. Support through simulations is now amenable for future developments.

Since the results obtained and the potential for improvement dis covered already suggest that magnetic chromatography is a potent way

to improve selectivity in specific particle size ranges of 10 nm to 1μm compared to conventional methods, the optimizations mentioned above are future research efforts.

## 5. Summary and conclusions

In this work, we propose a scheme to regard a novel multidimensional fractionation method, magnetic chromatography, numerically. For this type of chromatography, three mechanisms are essential for the size separation effect: the diffusion, the drag, and the magnetic force.

The model stated here is based on LBM and uses a simplified representation of the chromatographic column. We have shown that the ball matrix's actual porosity can be represented by a combination of the two nearest cubic unit cells, the primitive and body centered cubic. Additionally, the simulation is divided into a separate calculation for the fluid and the particle component. While we utilize the Navier Stokes and Ergun equation to solve the former, we utilize the ADE and the Stokes Einstein equation to describe the latter.

Primarily, the results of the developed method are compared with practical experiments. In this experimental series, we choose the particle radii 25 and 50 nm. Furthermore, we regard the case with and without a magnetic field of 0.85 mT. In order to enable comparison, an average transit time of the respective particle sizes is determined in practical and numerical experiments. Good agreement between the simulation results and the laboratory experiments is achieved. The absolute relative error is repeatedly smaller than 3%. The only exception is the case without a magnetic field and with a particle size of 25 nm. In this case, an error of about 5% is obtained.

This simulation successfully describes this multidimensional process. In particular, the simultaneous integration of the diffusion, magnetic, and drag force in a complex three dimensional space presents a novel challenge, which is solved using LBM. Overall, the simulation is a promising modeling process to investigate and develop further process optimizations of magnetic chromatography without high emerging costs. For example, a practically feasible separation matrix with optimized field gradients and magnetic properties is now numerically determinable. The proposed methods are also capable of modeling a scale up or investigate possible improvements of the separation by geometry changes.

## CRediT authorship contribution statement

**Jan E. Marquardt:** Conceptualization, Methodology, Software, Validation, Investigation, Writing original draft, Visualization. **Carsten-Rene Arlt:** Conceptualization, Methodology, Formal analysis, Investigation, Writing original draft, Visualization. **Robin Trunk:** Conceptualization, Methodology, Software, Writing review & editing, Supervision. **Matthias Franzreb:** Supervision, Funding acquisition, Project administration. **Mathias J. Krause:** Software, Supervision, Funding acquisition, Project administration.

## Acknowledgments

The authors would also like to thank the Steinbuch Centre for Computing at KIT for providing access to their high performance computer ForHLR II, where most computations were carried out as part of the CPE project.

The research leading to these results was supported by the German Research Foundation (DFG) [grants KR 4259/8 1 and FR 2131/6 1] within the priority program SPP2045 MehrDimPart "Highly specific and multidimensional fractionation of fine particle systems with technical relevance".

## References

[1] G. Goya, V. Grazu, M.R. Ibarra, Magnetic nanoparticles for cancer therapy, Curr. Nanosci. 4 (1) (2008) 1–16, http://dx.doi.org/10.2174/157341308783591861.

[2] J.W.M. Chon, C. Bullen, P. Zijlstra, M. Gu, Spectral encoding on Gold nanorods doped in a silica sol–gel matrix and its application to high-density optical data storage, Adv. Funct. Mater. 17 (6) (2007) 875–880, http://dx.doi.org/10.1002/adfm.200600565.

[3] A. Nasir, A. Kausar, A. Younus, A review on preparation, properties and applications of polymeric nanoparticle-based materials, Polym.-Plast. Technol. Eng. 54 (4) (2015) 325–341, http://dx.doi.org/10.1080/03602559.2014.958780.

[4] C.-R. Arlt, A. Tschöpe, M. Franzreb, Size fractionation of magnetic nanoparticles by magnetic chromatography, J. Magn. Magn. Mater. 497 (2020) 165967, http://dx.doi.org/10.1016/j.jmmm.2019.165967.

[5] T. Hahn, T. Huuk, V. Heuveline, J. Hubbuch, Simulating and optimizing preparative protein chromatography with chromx, J. Chem. Educ. 92 (9) (2015) 1497–1502, http://dx.doi.org/10.1021/ed500854a.

[6] S. Leweke, E. von Lieres, Chromatography analysis and design toolkit (CADET), Comput. Chem. Eng. 113 (2018) 274–294, http://dx.doi.org/10.1016/j.compchemeng.2018.02.025.

[7] Y. Yu, K.R. Wood, Y. Liu, Simulation and comparison of operational modes in simulated moving bed chromatography, Ind. Eng. Chem. Res. 54 (46) (2015) 11576–11591, http://dx.doi.org/10.1021/acs.iecr.5b02545.

[8] J. Lindner, K. Menzel, H. Nirschl, Simulation of magnetic suspensions for HGMS using CFD, FEM and DEM modeling, Comput. Chem. Eng. 54 (2013) 111–121, http://dx.doi.org/10.1016/j.compchemeng.2013.03.012.

[9] Y.S. Shaikh, C. Seibert, P. Kampeis, Study on optimizing high-gradient magnetic separation—Part 1: Improvement of magnetic particle retention based on CFD simulations, World J. Condens. Matter Phys. 6 (2) (2016) 123–136, http://dx.doi.org/10.4236/wjcmp.2016.62016.

[10] R. Gerber, M. Takayasu, F. Friedlaender, Generalization of HGMS theory: the capture of ultra-fine particles, IEEE Trans. Magn. 19 (5) (1983) 2115–2117, http://dx.doi.org/10.1109/TMAG.1983.1062795.

[11] M. Takayasu, R. Gerber, F. Friedlaender, Magnetic separation of submicron particles, IEEE Trans. Magn. 19 (5) (1983) 2112–2114, http://dx.doi.org/10.1109/TMAG.1983.1062681.

[12] K.C. Karki, E.R. Whitby, S.V. Patankar, C. Winstead, T. Ohara, X. Wang, A numerical model for magnetic chromatography, Appl. Math. Model. 25 (5) (2001) 355–373, http://dx.doi.org/10.1016/S0307-904X(00)00057-3.

[13] T. Ohara, S. Mori, Y. Oda, Y. Wada, O. Tsukamoto, Feasibility of magnetic chromatography for ultra-fine particle separation, IEEJ Trans. Power Energy 116 (8) (1996) 979–986, http://dx.doi.org/10.1541/ieejpes1990.116.8 979.

[14] H. Okada, K. Mitsuhashi, T. Ohara, E.R. Whitby, H. Wada, Computational fluid dynamics simulation of high gradient magnetic separation, Sep. Sci. Technol. 40 (7) (2005) 1567–1584, http://dx.doi.org/10.1081/SS-200056063.

[15] T. Henn, G. Thäter, W. Dörfler, H. Nirschl, M.J. Krause, Parallel dilute particulate flow simulations in the human nasal cavity, Comput. & Fluids 124 (2016) 197–207, http://dx.doi.org/10.1016/j.compfluid.2015.08.002.

[16] R. Trunk, T. Henn, W. Dörfler, H. Nirschl, M.J. Krause, Inertial dilute particulate fluid flow simulations with an Euler–Euler lattice Boltzmann method, J. Comput. Sci. 17 (2016) 438–445, http://dx.doi.org/10.1016/j.jocs.2016.03.013.

[17] S. Succi, The Lattice Boltzmann Equation: for Fluid Dynamics and Beyond, Oxford university press, 2001.

[18] T. Krüger, H. Kusumaatmaja, A. Kuzmin, O. Shardt, G. Silva, E.M. Viggen, The Lattice Boltzmann Method, Graduate Texts in Physics, Springer, 2017, http://dx.doi.org/10.1007/978-3-319-44649-3.

[19] V. John, E. Schmeyer, Finite element methods for time-dependent convection–diffusion–reaction equations with small diffusion, Comput. Methods Appl. Mech. Engrg. 198 (3–4) (2008) 475–494, http://dx.doi.org/10.1016/j.cma.2008.08.016.

[20] M. Augustin, A. Caiazzo, A. Fiebach, J. Fuhrmann, V. John, A. Linke, R. Umla, An assessment of discretizations for convection-dominated convection–diffusion equations, Comput. Methods Appl. Mech. Engrg. 200 (47–48) (2011) 3395–3409, http://dx.doi.org/10.1016/j.cma.2011.08.012.

[21] M.J. Krause, S. Avis, H. Kusumaatmaja, D. Dapalo, M. Gaedtke, N. Hafen, M. Haußmann, J. Jeppener-Haltenhoff, L. Kronberg, A. Kummerländer, J.E. Marquardt, T. Pertzel, S. Simonis, R. Trunk, M. Wu, A. Zarth, Openlb release 1.4: Open source lattice Boltzmann code, 2020, http://dx.doi.org/10.5281/zenodo.4279263.

[22] M.J. Krause, A. Kummerländer, S.J. Avis, H. Kusumaatmaja, D. Dapelo, F. Klemens, M. Gaedtke, N. Hafen, A. Mink, R. Trunk, J.E. Marquardt, M.-L. Maier, M. Haussmann, S. Simonis, Openlb—Open source lattice Boltzmann code, Comput. Math. Appl. (2020) http://dx.doi.org/10.1016/j.camwa.2020.04.033.

[23] S. Ergun, Fluid flow through packed columns, Chem. Eng. Prog. 48 (2) (1952) 89–94.

[24] Z. Guo, C. Zheng, B. Shi, Discrete lattice effects on the forcing term in the lattice Boltzmann method, Phys. Rev. E 65 (2002) 046308, http://dx.doi.org/10.1103/PhysRevE.65.046308.

[25] P.L. Bhatnagar, E.P. Gross, M. Krook, A model for collision processes in gases. I. Small amplitude processes in charged and neutral one-component systems, Phys. Rev. 94 (3) (1954) 511–525, http://dx.doi.org/10.1103/PhysRev.94.511.

[26] A.J.C. Ladd, Numerical simulations of particulate suspensions via a discretized Boltzmann equation. Part 1. Theoretical foundation, J. Fluid Mech. 271 (1994) 285–309, http://dx.doi.org/10.1017/S0022112094001771.

[27] A. Einstein, Über die von der molekularkinetischen Theorie der Wärme geforderte Bewegung von in ruhenden Flüssigkeiten suspendierten Teilchen, Ann. Phys. 322 (1905) 549–560.

[28] A.D. Ebner, J.A. Ritter, H.J. Ploehn, Feasibility and limitations of nanolevel high gradient magnetic separation, Sep. Purif. Technol. 11 (3) (1997) 199–210, http://dx.doi.org/10.1016/S1383-5866(97)00021-X.

[29] M. Franzreb, Magnettechnologie in der Verfahrenstechnik wässriger Medien, Universität Karlsruhe, 2003, http://dx.doi.org/10.5445/IR/200055719, 11.12.01; LK 01; Wissenschaftliche Berichte, FZKA-6916 (Oktober 2003) Habilitationsschrift, Universität Karlsruhe 2003.

[30] A.A. Mohamad, Lattice Boltzmann Method: Fundamentals and Engineering Applications with Computer Codes, second ed., Springer, London, 2019, http://dx.doi.org/10.1007/978-1-4471-7423-3.

[31] H.B. Huang, X.Y. Lu, M. Sukop, Numerical study of lattice Boltzmann methods for a convection–diffusion equation coupled with Navier–Stokes equations, J. Phys. A 44 (5) (2011) 055001, http://dx.doi.org/10.1088/1751-8113/44/5/055001.

[32] D. d'Humières, I. Ginzburg, Viscosity independent numerical errors for Lattice Boltzmann models: From recurrence equations to "magic" collision numbers, Comput. Math. Appl. 58 (2009) 823–840, http://dx.doi.org/10.1016/j.camwa.2009.02.008.

[33] J.D. Sterling, S. Chen, Stability analysis of lattice Boltzmann methods, J. Comput. Phys. 123 (1996) 196–206, http://dx.doi.org/10.1006/jcph.1996.0016.

[34] I. Ginzburg, Equilibrium-type and link-type lattice Boltzmann models for generic advection and anisotropic-dispersion equation, Adv. Water Resour. 28 (2005) 1171–1195, http://dx.doi.org/10.1016/j.advwatres.2005.03.004.

[35] I. Ginzburg, D. d'Humières, A. Kuzmin, Optimal stability of advection-diffusion lattice Boltzmann models with two relaxation times for positive/negative equilibrium, J. Stat. Phys. 139 (6) (2010) 1090–1143, http://dx.doi.org/10.1007/s10955-010-9969-9.

[36] R. Courant, E. Isaacson, M. Rees, On the solution of nonlinear hyperbolic differential equations by finite differences, Comm. Pure Appl. Math. 5 (3) (1952) 243–255, http://dx.doi.org/10.1002/cpa.3160050303.

[37] C. Horvath, S. Lipsky, Column design in high pressure liquid chromatography, J. Chromatogr. Sci. 7 (2) (1969) 109–116, http://dx.doi.org/10.1093/chromsci/7.2.109.

[38] K. Miyabe, Evaluation of chromatographic performance of various packing materials having different structural characteristics as stationary phase for fast high performance liquid chromatography by new moment equations, J. Chromatogr. 1183 (1–2) (2008) 49–64, http://dx.doi.org/10.1016/j.chroma.2007.12.064.

[39] O. Levenspiel, Chemical Reaction Engineering, third ed., Wiley, New York, 1999.

[40] P. Biehl, M. Von der Lühe, S. Dutz, F.H. Schacher, Synthesis, characterization, and applications of magnetic nanoparticles featuring polyzwitterionic coatings, Polymers 10 (1) (2018) 91, http://dx.doi.org/10.3390/polym10010091.

Karlsruher Institut für Technologie

OPEN ACCESS

# Repository KITopen

Dies ist ein Postprint/begutachtetes Manuskript.

Empfohlene Zitierung:

Marquardt, J. E.; Arlt, C.-R.; Trunk, R.; Franzreb, M.; Krause, M. J.
Numerical and experimental examination of the retention of magnetic nanoparticles in magnetic chromatography
2021. Computers and Mathematics with Applications, 89
doi: 10.554/IR/1000130899

Zitierung der Originalveröffentlichung:

Marquardt, J. E.; Arlt, C.-R.; Trunk, R.; Franzreb, M.; Krause, M. J.
Numerical and experimental examination of the retention of magnetic nanoparticles in magnetic chromatography
2021. Computers and Mathematics with Applications, 89, 34–43.
doi:10.1016/j.camwa.2021.02.010

**Lizenzinformationen: CC BY-NC-ND 4.0**